

SEISMIC BEHAVIOUR OF RC EXTERIOR WIDE BEAM-COLUMN JOINTS

S.H. LUK and J.S. KUANG

The Hong Kong University of Science and Technology, Hong Kong



SUMMARY:

The seismic behaviour of reinforced concrete exterior wide beam-column connections is investigated through computational simulations using ABAQUS. This study mainly focuses on the load transfer paths and different performances of the joints with conventional and wide beams. Wide beam-column connections with different beam widths and conventional beam-column joint specimens are simulated through three-dimensional analyses subjected to quasi-static cyclic loads. The numerical results show that wide beam-column joints have lower strengths and stiffness as compared to the conventional beam-column connection. It is found that lesser crack opening occurs in wide beam-column connections; hence less pinched hysteresis loops are observed. The beam width has significant effect on the load transfer paths in wide beam and joint core. The results also indicate that joint shear stress in wide beam-column connections is higher than that of conventional beam-column ones.

Keywords: Reinforced Concrete, Beam-Column Joints, Computational Simulations

1. INTRODUCTION

Reinforced concrete (RC) structures with wide and shallow beams provide different advantages and needs from construction and architectural points of view. A wide beam system may reduce the amount of formwork through repetition and then the construction cost can be greatly reduced and the construction works can be simplified. Furthermore, smaller storey height can be achieved from a wide beam system due to shallow beam depths (LaFave and White 1997). These advantages are well recognised for design of gravity load-resisting frames. However, the performance of wide beam structures subjected to seismic loads is not well understood since only limited experimental results are available currently as compared with those of conventional frame structures (Hatamoto et al. 1991; Popov et al. 1992; Gentry and Wight 1994; LaFave and White 1999; Benavent-Climent 2007; Benavent-Climent et al. 2009; Li and Kulkarni 2010). Hence, the use of wide beam systems in seismically active regions is usually prohibited.

Currently, many codes of practice restrict the use of a wide beam-column system to resist lateral loads through limiting the maximum beam width b_w . These geometric restrictions are based on historic design practice (LaFave and Wight 2001). In ACI-318, the beam width is limited to $b_c + 1.5h_b$, where b_c is the column width and h_b is the depth of wide beam. In New Zealand, the beam width is restricted to the lesser of $b_c + 0.5h_c$ and $2b_c$, where h_c is the column depth. In Eurocode 8, the width of primary beams should be smaller than the lesser of $b_c + h_b$ and $2b_c$. It can be seen that the restrictions of beam width vary with codes of practice, mainly because of the scattering experimental results. Therefore, more studies are required to identify an appropriate value for beam width restrictions.

The difference in seismic performance between a wide beam-column system and a conventional beam-column system is an essential factor that affects the use of wide beam systems in practice. It was indicated that the ultimate energy dissipation capacity of exterior wide beam-column connections was 2 to 15 times smaller than that of conventional sub-assemblages (Benavent-Climent 2007). On

the other hand, wide beam-column connections generally exhibit similar behaviour, in terms of energy dissipation and stiffness, to that of conventional beam-column connections (LaFave and Wight 2001). Anchorage conditions of beam longitudinal reinforcement has also shown to affect the seismic performance of wide beam-column assemblages (Hatamoto et al 1991). For wide beam-column systems, some beam bars are passing through or anchored inside the transverse beams, in which the anchorage conditions are general worse than that inside the joint cores. However, due to the lack of experimental data, the seismic behaviour of wide beam connections is still unclear. In order to utilise the beneficial effects of wide beam system in seismic regions, more studies in the area are needed.

Recently, same design methodologies have been adopted for conventional and wide beam-column assemblages except the geometric restriction, they may be over-simplified where the actual behaviour of wide beam-column assemblages, such as the complex load transfer mechanisms at regions adjacent to the joint cores and the effects of transverse beams to the overall performance, have been ignored. . A model is proposed to determine the nominal design capacities of wide beams (Benavent-Climent 2007), where the assumption is made that loading is transferred from the beam to the joint core via two load paths, named as inside beam portion and outside beam portion. However, the width of the inside beam portion is subjected to uncertainty.

This paper aims at investigating the seismic performance of wide beam-column assemblages through computational simulation using commercial software ABAQUS. Two wide beam-column connections with different beam widths and one conventional beam-column connection are studied under reversed cyclic loads. The hysteresis behaviour and load transfer mechanisms of wide beams systems are studied in detail.

2. PROTOTYPE MODELS

The geometry and reinforcement detailing of the prototype model, named as specimen EL tested by Benavent-Climent et al. (2009), is shown in Fig. 1. This specimen represents an exterior wide beam-column connection in the lower part of a typical RC frame structure constructed in past few decades in Spain. This model based on the assumption that the points of inflection under lateral loads are located at mid-span of beams and mid-storey height. The dimensions of primary beam, transverse beam and column are 480×180, 240×180 mm and 240×240 mm, respectively. 6-mm diameter stirrups with spacing 45 mm are provided on the transverse beams. A constant axial force of 214 kN (15% of column axial capacity) was applied on the column through two post-tensioned rods. Gravity loads acting on the wide beam was simulated by placing sand bags of total weight 40 kN at distance of 70 cm from the column axis. During the testing, the top end of the column was displaced in reversed cyclic manner, following the sequences of displacement $0.5\Delta_y$, $0.75\Delta_y$, $1.0\Delta_y$, $2.0\Delta_y$, $3.0\Delta_y$, $4.0\Delta_y$ and so up to a drift ratio of 8.0%, where Δ_y is equal to 2.5%. The nominal design flexural capacities of beam M_{fub}^+ and M_{fub}^- are 58.9 kNm, 94.2 kNm, respectively. The nominal design flexural capacities of column M_{fuc}^{top} and M_{fuc}^{bot} are 84.7 kNm and 93.1 kNm, respectively. The concrete cylindrical strength and steel yield stress are 24.9 MPa and 404 MPa, respectively. The beam width of this specimen is 480 mm which remains within the restriction in ACI-318-08 ($b_c + 1.5h_c = 600$ mm) but exceeds the limit in EC8 ($b_c + h_w = 420$ mm).

In this study, two specimens, including (1) conventional beam-column connection and (2) wide beam-column connection with different beam width b_w , are designed, so that the nominal design flexural capacities of beams and columns are approximately the same. The geometry and detailing of specimens 1 and 2 are shown in Fig. 2 and Fig. 3, respectively. Specimen 1 is a conventional beam-column connection with beam and column sizes of 240×400 mm and 240×240 mm, respectively. Specimen 2 is a wide beam-column connection with dimensions similar to Specimen EL except that the beam width is 720 mm, which exceeds the limits in both ACI-318-08 and EC8. Stirrups with diameter 6 mm and 55 mm spacing are provided in the transverse beams.

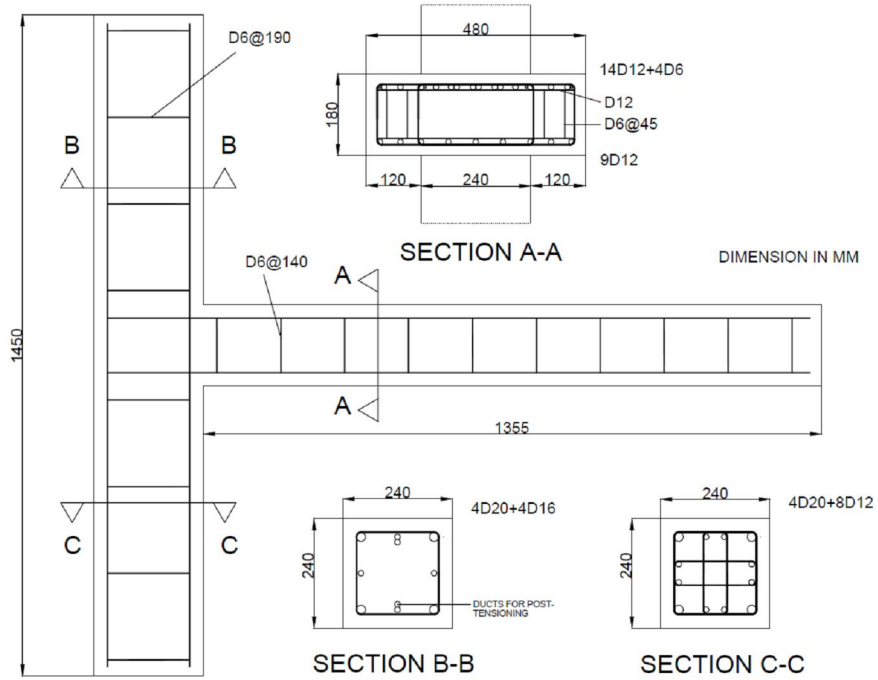


Figure 1. Prototype model (Specimen EL)

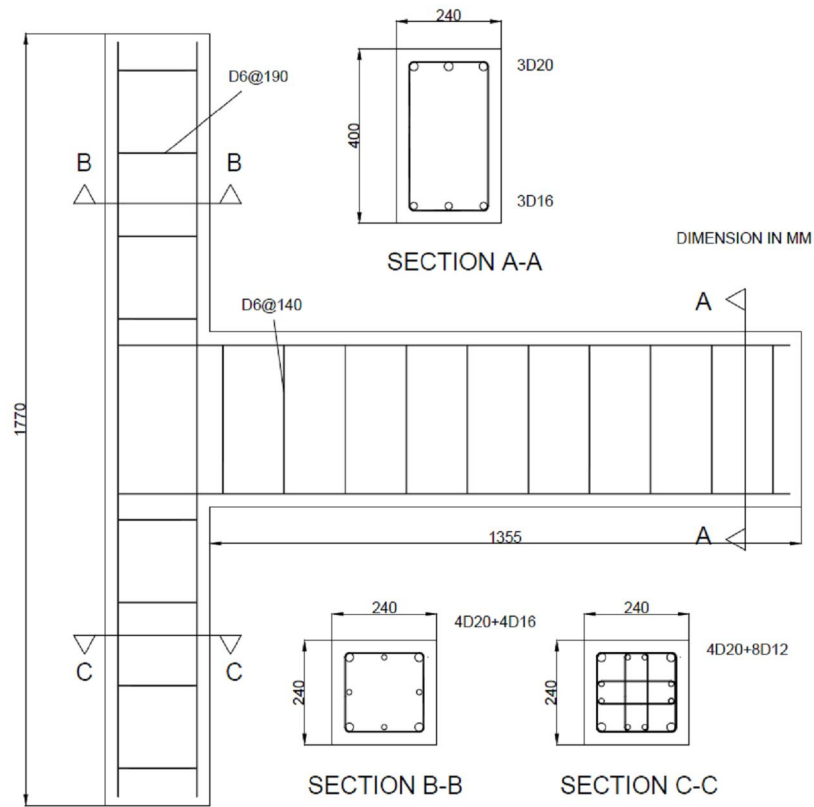


Figure 2. Conventional beam-column connection (Specimen 1)

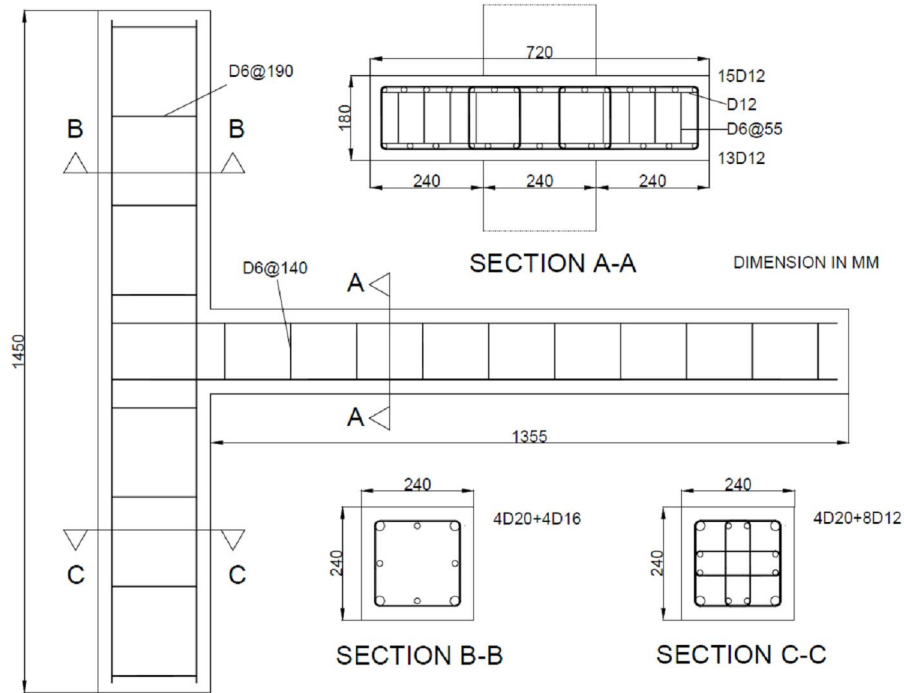


Figure 3. Wide beam-column connection (Specimen 2)

3. FINITE ELEMENT MODELS

3.1 Element Types

In the finite element models, concrete is modelled with linear 8-node, 3-D solid elements (C3D8R). The reduced integration technique, which uses a lower-order integration to form the element stiffness, is adopted to eliminate the locking behaviour resulted from the first-order elements, and the enhanced hourglass control, which introduces a small amount of hourglass stiffness based on ‘enhanced assumed strain field’, is used to suppress the zero-energy modes resulted from the reduced integration technique. Longitudinal reinforcement and stirrups are modelled with linear 2-node, 3-D truss elements (T3D2) which are embedded in the concrete element. Cohesive surfaces are defined inside the joint cores to model the propagation of diagonal cracks under reversed cyclic loads. Note that many experimental findings have indicated that the diagonal cracks play a significant role in the seismic behaviour of the joint cores. After carrying out mesh sensitivity studies, average mesh size of 50mm is adopted for the models, as shown in Fig. 4. The homogeneous mechanical properties of continuum body are described within a volume called representative volume element (RVE) (Lemaitre, 1992).

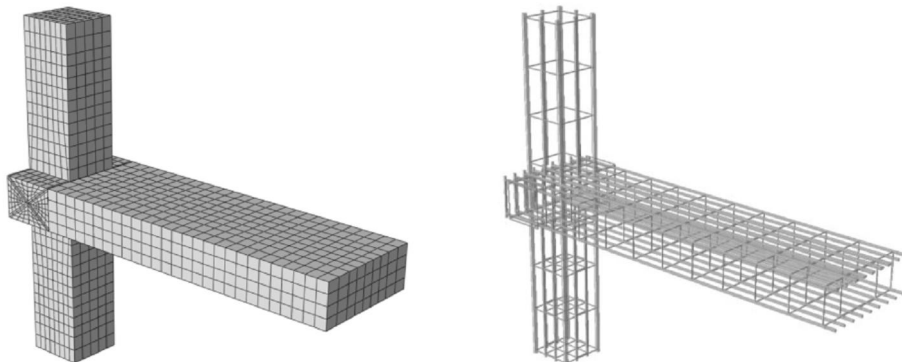


Figure 4. Finite element model of Specimen EL

3.2 Material models

Concrete Damaged Plasticity Model (Lubliner et al. 1989; Lee and Fenves 1998) is used as the constitutive model for concrete material. This model composes of the concepts of non-associated multi-hardening plasticity and scalar damaged elasticity to describe the non-linear, irreversible and softening phenomena of concrete subjected to general loadings. The yield function in the model is defined as

$$F(\bar{\sigma}, \tilde{\varepsilon}^{pl}) = \frac{1}{1-\alpha} (\bar{q} - 3\alpha\bar{p} + \beta(\tilde{\varepsilon}^{pl}) \langle \hat{\sigma}_{\max} \rangle - \gamma \langle -\hat{\sigma}_{\max} \rangle) - \bar{\sigma}_c(\tilde{\varepsilon}^{pl}) \quad (3.1)$$

where \bar{p} and \bar{q} are the effective hydrostatic stress and Mises equivalent effective stress, respectively; is the algebraically maximum eigenvalue of effective stress tensor; and α , β and γ are the parameters that control the shape of the yield surface in stress space. The flow rule is non-associated and the flow potential is taken as Drucker-Prager hyperbolic function,

$$G = \sqrt{(e\sigma_{t0} \tan\varphi)^2 + \bar{q}^2} - \bar{p} \tan\varphi \quad (3.2)$$

where φ is the dilation angle measured in the p - q plane at high confining pressure; σ_{t0} is the uniaxial tensile stress at failure; and e is the eccentricity defining the rate at which the function approaches the asymptote so that the flow potential tends to linear Drucker-Prager flow potential as the eccentricity tends to zero. The stress-strain relationships for concrete in both tension and compression were modelled based on the CEB-FIP Model Code. In addition, fracture energy in tension and compression are introduced as material parameters in order to tackle the mesh sensitivity and localization issues in the numerical simulations (Krätzig et al., 2004). Material parameters of concrete are that compressive strength is 25 MPa, tensile strength is 2.5 MPa, Young's modulus is 30 GPa, Poisson ratio is 0.2, density is 2400 kg/m³, dilation angle is 30°, flow potential eccentricity is 0.1, biaxial/uniaxial compression strength ratio is 1.16 and deviatoric stress invariant ratio is 2/3.

Monti-Nutti model (Monti and Nutti, 1992) is adopted for steel material. This model consists of four sets of hardening rules, including kinematic hardening rule, isotropic hardening rule, memory rule and saturation rule to characterise the inelastic behaviour of steel reinforcing bars. Most of the major inelastic behaviour, such as strain hardening and Bauschinger effect, can be handled by this model. Furthermore, inelastic buckling of reinforcing bars, which is commonly found in non-seismically designed RC structures under compression, can be well considered. Two sets of equation are provided for updating the internal parameters for the absence and presence of buckling. Material parameters of steel are that Young's modulus is 200 GPa, Poisson ratio is 0.3, density is 7800 kg/m³, yield stress is 400 MPa, hardening parameter b is 0.02 and initial curvature parameter R_0 is 20. Two additional parameters, A_1 and A_2 are taken as 18 and 0.005, respectively.

The two major diagonal cracks inside the joint cores are modelled through surface-based cohesive behaviour (Hillerborg et al. 1976). This model consists of two parts, including linear elastic relationship and interface traction-separation constitutive law in order to characterise both the pre-peak and post-peak behaviour of cracked concrete. The major parameters include the tensile strength of concrete, fracture energy. In this study, maximum stress criterion is adopted as the damage initiation model, while energy-based linear damage evolution law is chosen as the traction-separation relationship in post-cracking region. The mixed mode behaviour is described using the Power law. In the cohesive model, the maximum tensile stress is 2.5 MPa and the fracture energy is 0.17 N/mm.

3.3 Boundary Conditions

The boundary conditions of the finite element models are shown in Fig. 5. Pin support and roller support with free translational movement along the column axis are imposed on the bottom end and upper end of column, respectively. The loading schedule in this study includes two steps. First,

constant column axial load is applied at the top of the column. Second, the bottom end of the column is displaced laterally following the pattern as shown in Fig. 5 to simulate the working condition of the beam-column assemblies under load reversals.

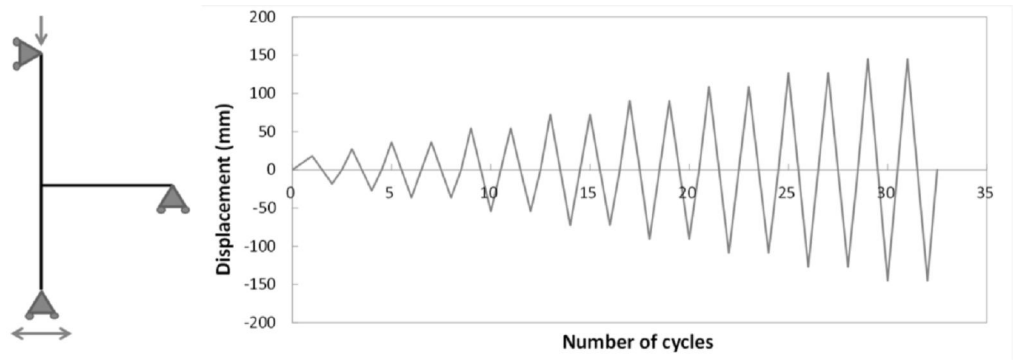


Figure 5. Boundary conditions and loading schedule

4. RESULTS AND DISCUSSIONS

4.1 Comparison between Experimental and Numerical Results

Fig. 6 shows the force-displacement relationships of Specimen EL obtained through the numerical simulation in this study and the experiment by Benavent-Climent et al. (2009). It can be seen that the overall trend of Specimen EL obtained through the numerical simulation is similar to that of the experiment. The numerical model slightly over-estimates the peak strength of Specimen EL in positive and negative loading directions. Both results show similar post-peak softening behaviour.

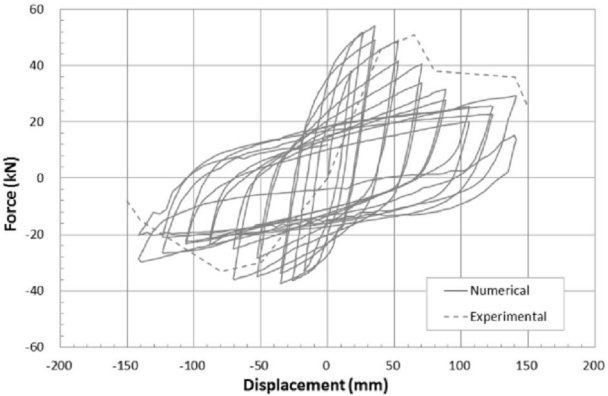


Figure 6. Comparison between numerical results and experimental finding

4.2 General Behaviour

From Fig. 6, it can be seen that the hysteresis loops of Specimen EL shows slightly pinching and early degradation. This specimen reaches its peak strengths of 53.93 kN and -37.34 kN in positive and negative directions at inter-storey drift ratio of 2.5%. Strength degradation is observed for drift ratios beyond this value due to the damage and opening of diagonal cracks inside the joint core and transverse beams. The load capacity reduce to 0.75 time of the original value at inter-storey drift ratio about 3.5%.

The hysteresis behaviour of Specimens 1 and 2 are shown in Fig. 7(a) and Fig. 7(b), respectively. From Fig. 7(a), it is seen that Specimen 1 exhibits severe pinching hysteresis behaviour and less ductility as compared with Specimen EL. The peak strengths of Specimen 1 in positive and negative

directions are 75.93 kN and -49.37 kN, respectively. Strength degradation is found for the drift ratio exceeding 2.5%. In addition, Specimen 1 can survive only up to inter-storey drift ratio of 7.5%, since the diagonal cracks inside the joint core open extensively, resulting in completely loss of structural integrity.

For Specimen 2, the hysteresis behaviour is similar to that of Specimen EL, which shows slightly pinching effect and early strength degradation. The peak strengths of this specimen in positive and negative directions are 58.42 kN and -52.22 kN, respectively. The high capacity in negative direction is appeared in Specimen 2 mainly because of the additional flexural reinforcement in the wide beam for the crack control purpose.

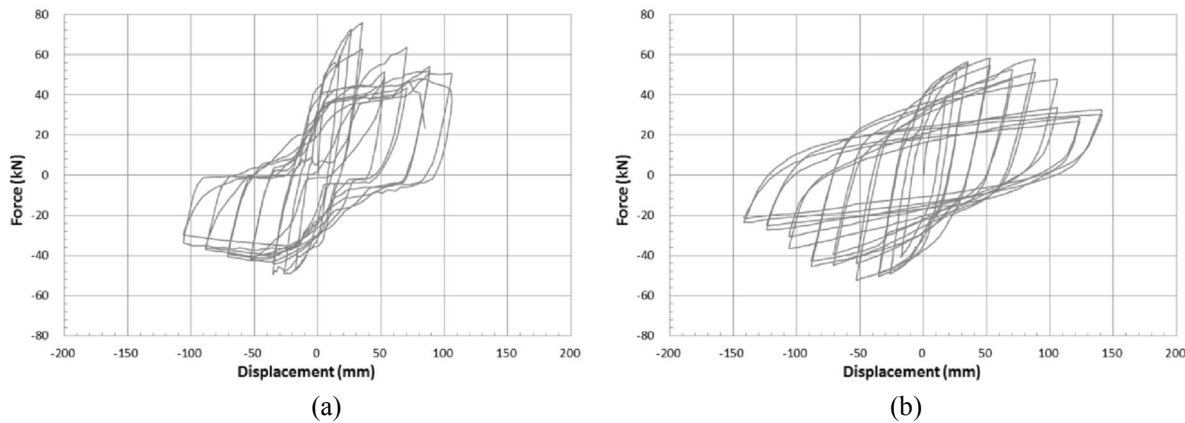


Figure 7. Hysteresis behaviour obtained from numerical simulations: (a) Specimen 1; (b) Specimen 2

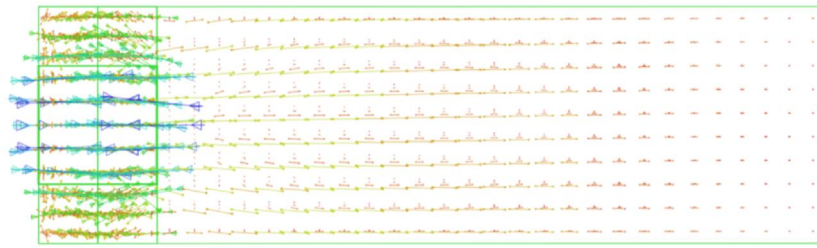
4.3 Comparisons between Specimens

4.3.1. Differences between conventional and wide beam-column assemblages

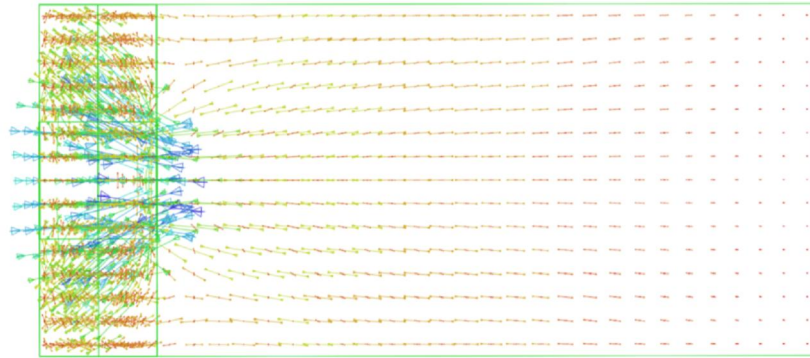
It is shown in Fig. 6 and Fig. 7(a) that the conventional beam-column assemblage exhibits severe pinching hysteresis loops, as compared with that of wide beam-column assemblage. This is because the crack opening-closing effect takes place extensively in Specimen 1 but not in Specimen EL. In addition, the crack width in Specimen 1 is larger than that in Specimen EL at the same drift ratios. This phenomenon is possibly due to the difference in orientations of diagonal cracks inside the joint cores. For the conventional beam-column assemblage, the angle of inclination of diagonal cracks from horizontal axis is deeper than that of wide beam-column assemblage. In such case, the crack closing effect resulting from the column axial load becomes smaller. The column axial load may even tend to shear the concrete elements apart between the crack interfaces. On the other hand, the small inclination of diagonal cracks in Specimen EL is not favourable for the formation of shear crack. Furthermore, the well reinforced transverse beams can provide additional confining effects to the joint cores to prevent opening of diagonal cracks. Although Specimen 1 has severe pinching hysteresis behaviour due to crack opening and closing effect, it is possible to reach higher capacity and secant stiffness in both positive and negative loading directions, as compared with those of Specimen EL.

4.3.2. Effects of beam width

Fig. 8 represents the concrete compressive stress trajectories for Specimen EL and Specimen 2 at inter-storey drift ratio of 2.5%. For Specimen EL, the stress distribution on the portion of wide beam outside the column width is quite regular and almost along the beam axis, except that a small inclination of load path is observed at regions close to the column. For Specimen 2, however, the stress distribution in the exterior portion of wide beam is extremely non-uniform. Part of the loading in this region is transferred to the beam-column joint directly through the diagonal paths with an angle 40° to the beam axis. The remaining portion of loading passes towards the transverse beams first, and then transfers to the joint core through torsion. The change of load paths with beam width may possibly affect the load transfer mechanisms of the joint core.



(a)



(b)

Figure 8. Load transfer paths in concrete for wide beam-column connections: (a) Specimen EL; (b) Specimen 2

Fig. 9 shows the stress distribution in tension reinforcement for Specimen EL and Specimen 2 at inter-storey drift ratio of 2.5%. Fig. 9(a) shows that all tension bars on the wide beam have similar behaviour when the width of exterior portion is $0.5h_c$, except that yielding of tension reinforcement within the column width occurs first. For Specimen 2, the tension reinforcement on the portion outside the column width behaves different to that within the column width, as shown in Fig. 9(b). For the reinforcement located beyond distance $0.5h_c$ from the column, the tension zones shift away from the beam-column interfaces. This is because the diagonal compression stress fields are developed in the exterior portion of wide beam, as shown in Fig. 8(b). This compression force in the wide beam must be balanced by the tension force developed in reinforcement, resulting in such a stress distribution in tension reinforcement. This observation is important for understanding the load transfer mechanism in a wide beam system.



(a)

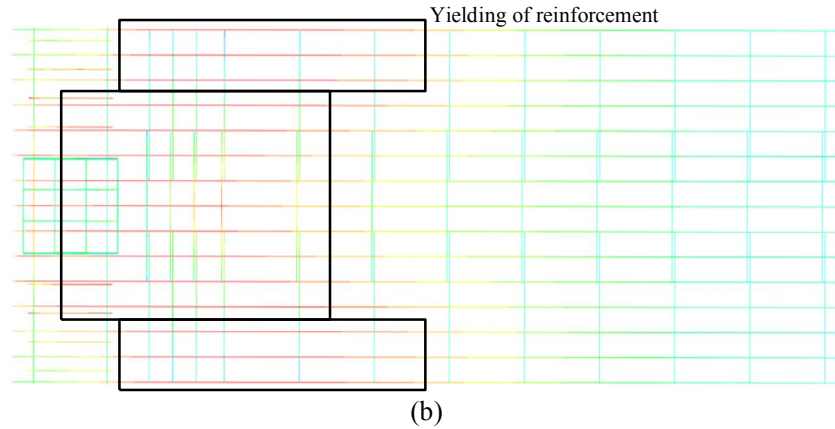


Figure 9. Stresses in tension reinforcement for wide beam-column connections: (a) Specimen EL; (b) Specimen 2

4.4 Joint Behaviour

The average nominal joint shear stress, which is defined as $v_{jh}/\sqrt{f_c}$, based on the cross-sectional area of column for Specimen EL, Specimen 1 and Specimen 2 are 0.8, 0.65 and 0.94, respectively. It is clearly seen that wide beam-column assemblages can achieve higher joint shear stresses, as compared with that of conventional beam-column assemblage. This result is obvious because lesser diagonal crack opening is found in wide beam-column assemblages due to small diagonal crack inclinations. The confining effect provided by transverse beams is may also enhance the joint behaviour.

Fig. 10 shows the load transfer paths in the joint cores and transverse beams at the stage of the maximum joint shear stress. These figures indicate that the exterior portion of wide beam can resist beam shear through the formation of concrete struts and tension ties. In addition, the orientation of concrete struts in the transverse beams is affected by the beam width. For specimen EL, concrete diagonal struts in the transverse beams have almost the same orientation to that inside the joint core. For specimen 2, however, concrete diagonal struts in the transverse beams direct towards the column, forming an angle of 40° with the beam axis. In this case, a tension tie along the transverse beam axis must be developed in order to maintain force equilibrium. On the other hand, cracking of transverse beams is not severe in this study, since the concrete is well confined by closely spaced stirrups.

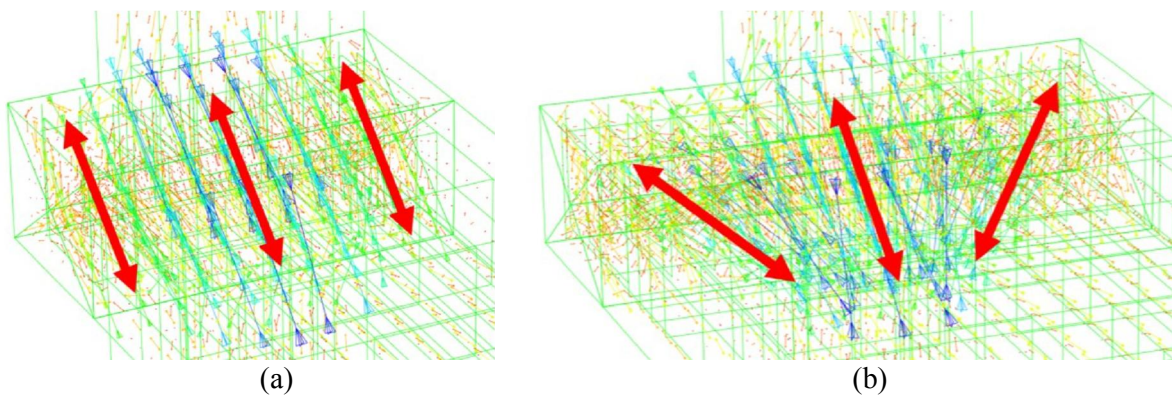


Figure 10. Load transfer paths in beam-column joints: (a) Specimen EL; (b) Specimen 2

5. CONCLUSIONS

The seismic behaviour of two wide beam-column connections and one conventional beam-column connection have been investigated in this study through computational simulations. Based on the numerical results, the following conclusions can be drawn.

1. The conventional beam-column connection has higher strength and secant stiffness, as compared with wide beam-column connections. On the other hand, the conventional beam-column connection exhibits severe pinching and less deformability due to the crack opening and closing effect, while this effect is not significant in well reinforced wide beam-column connections.
2. The load transfer paths in wide beams depend largely on the width of the beam. For a small beam width ($b_w \leq b_c + h_c$), both the exterior and interior portions of wide beams exhibit similar performance. For a large beam width ($b_w > b_c + 2h_c$), part of the loading is transferred to the joint core directly, while the remaining part is transferred towards the transverse beams. Therefore, the demands of tension reinforcement in wide beams are not uniform.
3. The joint shear stress in wide beam-column connections is generally higher than that of conventional beam-column connections since lesser diagonal cracks are found inside the joint cores of wide beam-column connection due to the small inclination of crack angles and the confining action provided by the transverse beams.
4. The orientations of concrete diagonal struts inside the joint core and transverse beams change with beam width. This will affect the development of strut-and-tie model for determining the specimen capacity.

AKNOWLEDGEMENT

The support of Hong Kong RGC under grant No. 614011 is gratefully acknowledged.

REFERENCES

- ABAQUS, INC. (2010). ABAQUS analysis user's manual: version 6.10. Providence (RI).
- ACI Committee 318. (2007). Building Code Requirements for Structural Concrete (ACI 318-08) and Commentary. American Concrete Institute, Farmington Hills, Michigan.
- CEN. (2004). Eurocode 8: Design of Structures for Earthquake Resistance - Part 1: General Rules, Seismic Actions and Rules for Building. European Committee for Standardization.
- Benavent-Climent, A., Cahís, X. and Zahran, Z. (2009). "Exterior wide beam-column connections in existing RC frames subjected to lateral earthquake loads". *Engineering Structures*, **31:7**, 1414-1424.
- Comité Euro-International du Béton. (1993). CEB-FIP Model Code 1990. Thomas Telford Services Ltd.
- Hillerborg M., Modeer, M. and Peterson, P. (1976). "Analysis of crack formation and crack growth in concrete by means of fracture mechanics and finite elements". *Cement and Concrete Research*, **6**, 773-782.
- Krätzig W.B. and Pölling R. (2004). "An elasto-plastic damage model for reinforced concrete with minimum number of material parameters". *Computers and Structures*, **82:15-16**, 1201-1215.
- Lee J. and Fenves G.L. (1998). "Plastic-damage model for cyclic loading of concrete structures". *Journal of Engineering Mechanics*, **124:8**, 892-900.
- Lubliner J., Oliver J., Oller S. and Onate E. (1989). "A plastic-damage model for concrete". *International Journal of Solids and Structures*, **25:3**, 229-326.
- Benavent-Climent A. (2007). "Seismic behaviour of RC wide beam-column connections under dynamic loading". *Journal of Earthquake Engineering*, **11:4**, 493-511.
- Benavent-Climent A., Cahís X. and Zahran R. (2009). "Exterior wide beam-column connections in existing RC frames subjected to lateral earthquake loads". *Engineering Structures*, **31:7**, 1414-1424.
- Gentry R.G. and Wight J.K. (1994). "Wide beam-column connections under earthquake-type loading". *Earthquake Spectra*, **10**, 675-703.
- Hatamoto H., Bessho S. and Matsuzaki Y. (1991). "Reinforced concrete wide-beam-to-column subassemblages subjected to lateral load". *American Concrete Institute*, SP123-11, **123**, 291-316.
- Li B. and Kulkarni S.A. (2010). "Seismic behaviour of reinforced concrete exterior wide beam-column joints". *Journal of Structural Engineering*, **136:1**, 26-36.
- LaFave J.M. and Wight J.K. (2001). "Reinforced concrete wide beam-column connections vs. conventional construction: Resistance to lateral earthquake loads". *Earthquake Spectra*, **17**, 479-505.
- Monti G. and Nutti C. (1992). "Nonlinear behaviour of reinforcing bars including buckling". *Journal of Structural Engineering*, **118:12**, 3268-3284.
- NZS 3101. (2006). Concrete Structures Standard Part. Part 1: The Design of Concrete Structures & Part 2: Commentary on the Design of Concrete Structures. Standards New Zealand, Wellington.
- Popov E.P., Cohen J.M., Koso-Thomas K. and Kasai K. (1992). "Behavior of interior narrow and wide beams". *ACI Structural Journal*, **89:6**, 607-616.